aTelethon Institute for Gene Therapy (SR-Tiget), Division of Regenerative Medicine, Stem Cells, and Gene Therapy, IRCCS San Raffaele Scientific Institute, Milan, Italy; bUOS Milano, IRGB CNR, Milan, Italy; cLaboratory of Bioceramics and Bio-Hybrid Composites, Institute of Science and Technology for Ceramics (ISTEC), National Research Council (CNR), Faenza, Italy; dHumanitas Clinical and Research Center, Rozzano, Milan, Italy; eVita-Salute San Raffaele University, Milan, Italy; fPaediatric Immunohematology and Bone Marrow Transplantation Unit, IRCCS San Raffaele Scientific Institute, Milan, Italy; gPreclinical Imaging Facility, Experimental Imaging Center, IRCCS San Raffaele Scientific Institute, Milan, Italy; hPaediatric Immunology, Department of Biomedicine, University of Basel, Basel, Switzerland; iDevelopmental Immunology, Weatherall Institute of Molecular Medicine, University of Oxford, Oxford, United Kingdom

Correspondence: Marita Bosticardo, Ph.D., Laboratory of Clinical Immunology and Microbiology, IDGS, DIR, NIAID, NIH, DHHS, 10 Center Drive, Bldg. 10 CRC, Room 5W3840, Bethesda, MD 20892-1456, USA. Telephone: 001-240-292-4727; e-mail: marita.bosticardo@nih.gov

# Gene Modification and Three-Dimensional Scaffolds as Novel Tools to Allow the Use of Postnatal Thymic Epithelial Cells for Thymus Regeneration Approaches

ILEANA BORTOLOMAI [ID],a,b MONICA SANDRI,c ELENA DRAGHICI,a ELENA FONTANA,b,d ELISABETTA CAMPODONI,c GENNI ENZA MARCOVECCHIO,a FRANCESCA FERRUA,a,e,f LAURA PERANI,g ANTONELLO SPINELLI,g TAMARA CANU,g MARCO CATUCCI,h TIZIANO DI TOMASO,a LUCIA SERGI SERGI,a ANTONIO ESPOSITO,e,g ANGELO LOMBARDO,a,e LUIGI NALDINI,a,e ANNA TAMPIERI,c GEORG A. HOLLANDER,h,i ANNA VILLA,a,b MARITA BOSTICARDOa

**Key Words.** 3D collagen scaffolds • Lentiviral vector • Thymic epithelial cells • Thymic regeneration

## ABSTRACT

Defective functionality of thymic epithelial cells (TECs), due to genetic mutations or injuring causes, results in altered T-cell development, leading to immunodeficiency or autoimmunity. These defects cannot be corrected by hematopoietic stem cell transplantation (HSCT), and thymus transplantation has not yet been demonstrated to be fully curative. Here, we provide proof of principle of a novel approach toward thymic regeneration, involving the generation of thymic organoids obtained by seeding gene-modified postnatal murine TECs into three-dimensional (3D) collagen type I scaffolds mimicking the thymic ultrastructure. To this end, freshly isolated TECs were transduced with a lentiviral vector system, allowing for doxycycline-induced Oct4 expression. Transient Oct4 expression promoted TECs expansion without drastically changing the cell lineage identity of adult TECs, which retain the expression of important molecules for thymus functionality such as Foxn1, Dll4, Dll1, and AIRE. Oct4-expressing TECs (iOCT4 TEC) were able to grow into 3D collagen type I scaffolds both in vitro and in vivo, demonstrating that the collagen structure reproduced a 3D environment similar to the thymic extracellular matrix, perfectly recognized by TECs. In vivo results showed that thymic organoids transplanted subcutaneously in athymic nude mice were vascularized but failed to support thymopoiesis because of their limited in vivo persistence. These findings provide evidence that gene modification, in combination with the usage of 3D biomimetic scaffolds, may represent a novel approach allowing the use of postnatal TECs for thymic regeneration. STEM CELLS TRANSLATIONAL MEDICINE 2019;8:1107–1122

## SIGNIFICANCE STATEMENT

Transient Oct4 expression promoted thymic epithelial cells expansion without changing the cell lineage identity of adult thymic epithelial cells (TECs). iOCT4 TECs were able to expand into three-dimensional (3D) collagen-scaffolds both in vitro and in vivo, demonstrating that the collagen structure reproduced a 3D environment similar to the thymic extracellular matrix, perfectly recognized by TECs. Thymic organoids transplanted subcutaneously in athymic nude mice were vascularized, which showed a mild short-term thymopoietic activity. These findings provide evidence that gene modification, in combination with the usage of 3D biomimetic scaffolds, represents a novel approach that would allow the use of postnatal TECs in thymic regeneration.

## INTRODUCTION

The thymus is a primary lymphoid organ that represents a crucial component of the adaptive immune system, since the specialized thymic microenvironment sustains the development of a broad repertoire of self-tolerant T lymphocytes [1, 2]. Its function is fundamental for mounting an immune response against pathogens and tumors, but it is also important for the establishment of central tolerance. Several factors including aging, viral infections, chemotherapy, and radiotherapy contribute to thymus involution [3, 4]. Therefore, thymic dysfunctions caused

by physiological processes or by external stimuli render patients extremely vulnerable to infections, malignancies, and autoimmune diseases [5, 6].

Many research groups have primarily focused on finding possible strategies to rejuvenate the thymus and have developed promising therapeutic approaches to target unsuccessful thymopoiesis, post-transplant immunodeficiency, and infection-related morbidity and mortality after HSCT [7, 8]. However, a few molecules and genes, such as keratin growth factor, Interleukin (IL)22, IL7, and Foxn1, have been identified as key players of the mechanistic pathway for endogenous thymic regeneration [9–13]. Growth factors and hormone therapies were also explored in order to restore age-related or injury-related thymic degeneration, but, despite encouraging results, they have short-term effects and/or require a recurrent administration, which is complicated by their toxic effects on other tissues and organs [14, 15].

Thymus transplantation represents another promising alternative to complement bone marrow transplantation or to treat congenital thymic anomalies, but T-cell reconstitution following thymus grafting is frequently incomplete and transient, complicated by a skewed T-cell receptor repertoire and an increased occurrence of autoimmunity [16, 17].

The thymus is anatomically organized into two discrete cortical and medullary regions, containing phenotypically and functionally distinct thymic epithelial cells (TECs), named medullary TECs (mTECs) and cortical TECs (cTECs). The unique architecture of the thymic stroma is essential for TEC development and function as well as for the maturation and selection of a self-tolerant T-cell repertoire [18]. Differently from the epithelium of other organs, the thymic microenvironment is structured as a three-dimensional (3D) network in which crosstalk of TECs and thymocytes takes place [2].

The field of tissue engineering has put considerable efforts into the development of materials and techniques for the in vitro generation of tissues of clinical relevance [19, 20]. The major challenge for tissue engineering is to successfully recreate the complexity of the 3D structure of the thymic microenvironment and to fully rebuild the composition and organization of the thymic extracellular matrix (ECM). The use of thymic organoids formed by human TECs and fibroblasts as well as seeding TECs into matrigel or other 3D biocompatible systems has been shown to promote a transient thymopoiesis in vivo [11, 21]. The use of decellularized thymic tissue has been suggested to overcome these limitations and has shown promising results in mouse models [22]. However, the use of decellularized tissues, obtained from cadavers or patients undergoing cardiothoracic surgery, limits the applicability of such approaches to the availability of donors.

The use of postnatal TECs for thymic regeneration has revealed challenging because of the loss of thymopoietic function of TECs after in vitro culture and their inability to reaggregate after isolation [23]. Recent studies have used several approaches that could overcome this barrier, including the identification of thymic epithelial progenitor cells (TEPCs) or the differentiation of embryonic stem cells or induced pluripotent stem (iPS) cells into TEPC, but they have all some limitations for clinical purposes [24–26]. To avoid the use of embryonic TECs or iPS-derived TECs, attempts have been made by combining mature TECs with different 3D systems for developing functional mini-thymus units [27–29]. Several studies have been focused on the investigation

of ideal biomaterials for human applicability [30, 31], which need to be biocompatible, biodegradable, and easily detectable with imaging techniques regularly used in standard clinical practice. Collagen has been widely used in tissue engineering because it can be assembled in fibers closely reproducing the chemical and morphological characteristics of those present in soft tissues [32, 33]. Therefore, the production of collagen porous biomatrix could make this biomaterial suitable for the generation of thymic constructs.

Hence, we developed a potentially new therapeutic strategy that foresees transplantation of biomimetic scaffolds, mimicking the thymic ECM organization, obtained by seeding adult murine TECs and expanding them into 3D collagen type I scaffolds. In order to use postnatal TECs for the generation of transplantable thymic structure, we sought to induce a short-term expression of Oct4, a transcription factor involved in the maintenance or induction of pluripotency in embryonic cells [34, 35], to obtain transient partial de-differentiation and promote their expansion. To create a physiologically relevant microenvironment to seed TECs, we tested 3D collagen type I scaffolds crosslinked with different amounts of 1,4-butanediol diglycidyl ether (BDDGE; 3%–5%). Here, we show that 3% BDDGE collagen-based scaffolds seeded with gene-modified TECs and transplanted subcutaneously in athymic nude mice were perfused and colonized by small new blood vessels and were able to sustain TEC survival in a 3D microenvironment. However, further improvement of the 3D scaffold composition is required to obtain long-term in vivo persistence of organoids that could allow the development of this approach for future clinical applications.

## MATERIALS AND METHODS

### Animals

Wild-type (WT) C57BL/6 (B6) and CD1 athymic nude mice were purchased from Charles River Laboratories, Inc. (Calco, Italy) and housed under specific pathogen-free conditions at the San Raffaele Hospital Animal Facility. This study was carried out in accordance with the recommendations of the Italian Ministry of Health. The protocol was approved by the Animal Care and Use Committee of the San Raffaele Scientific Institute (IACUC 712). For TEC isolation, we used B6 mice ranging from 4 to 6 weeks old. For scaffolds transplantation, we used CD1 athymic nude mice from 6 to 10 weeks old, unless otherwise stated.

### TEC Isolation, Enrichment, and Culture

Thymus was isolated from 4- to 6-week-old WT mice. Thymus was cleaned up from fat and stromal tissues under the microscope and then digested at 37°C (three steps of 5 minutes) with a solution containing Liberase (Roche, Germany) and DNAse I (Roche). Digested thymus was recovered in Iscove medium (Sigma–Aldrich, Germany) supplemented with 10% fetal bovine serum (FBS; Euroclone, Italy), 1% penicillin/streptomycin (Lonza, Switzerland), and 2% glutamine (Lonza). TECs were further enriched by depleting CD45+ cells with the AutoMACS Separator (Miltenyi Biotec, Germany) after incubating thymic cells with anti-CD45 microbeads (Miltenyi Biotec). The purity of enriched TECs (CD45-EpCam+) was then checked by multicolor flow cytometric analyses. Enriched TECs were cultured in CnT-57.S (CELLnTEC Advanced Cell Systems, Switzerland) supplemented

with Rho-associated, coiled-coil containing protein kinase (ROCK) inhibitor 1 µg/ml (Y-27632, Merck Millipore) for 7–9 days after isolation; afterward, culture medium was switched to X-VIVO10 (Lonza) supplemented with the ROCK inhibitor.

### Lentiviral Vector Production and TEC Transduction

Third-generation lentiviral vectors (LVs) were produced by $Ca_3PO_4$ cotransfection of four plasmids into 293 T cells. Supernatants were collected, passed through a 0.22 µm filter, and purified by ultracentrifugation as described [36]. Titer was estimated measuring vector particles by Human Immunodeficiency Virus-1Gag p24 antigen immunocapture (MEN Life Science Products) and Quantitative Real-Time Polymerase Chain Reaction (PCR) on Viia7 PCR system (Applied Biosystems, Waltham, MA) was used to quantify vector copy number/genome as previously described [37]. Genomic DNA was extracted with QIAamp DNA blood mini kit (QIAGEN, Germany) according to manufacturer's instructions. Vector infectivity was calculated as the ratio between titer and p24. For concentrated pCCLsin.PPT.hPGK.GFP.Wpre_mut_AMP LV (from now on PGK.GFP LV), titer ranged from $1 \times 10^9$ to $1 \times 10^{11}$ transducing units (TU)/ml; for concentrated hPGK.rtTAm2v10.WPRE.minhCMV.mCHERRY.SV40PA LV (from now on rtTA.mCherry LV), titer ranged from $1.32 \times 10^9$ to $4.8 \times 10^9$ TU/ml; and for pCCL.sin.cPPT.SK-T6.GFP-OCT4.WPRE LV (from now on iOCT4 LV), titer ranged from $2.74 \times 10^9$ to $2 \times 10^{10}$ TU/ml.

Two days after isolation, TECs were transduced with the rtTA.mCherry LV at multiplicity of infection (MOI) 0.5 in CnT-57.S medium supplemented with ROCK inhibitor and Polybrene 8 µg/ml (Sigma–Aldrich). Medium was changed 24 hours later. At day 4, TECs were transduced with the Oct4.vexGFP LV at MOI 0.5 in CnT-57.S medium supplemented with ROCK inhibitor and Polybrene and medium was changed 24 hours later. For standard culture, the medium was changed every other day. Doxycycline hyclate (D9891, Sigma–Aldrich; 0.01 µg/ml) was added starting at day 5 after isolation. TECs were cultured in CnT-57.S supplemented with ROCK inhibitor until day 7–9 after isolation; afterward, the medium was switched to X-VIVO10 medium supplemented with the ROCK inhibitor.

### Preparation and Chemical Characterization of BDDGE Scaffolds

Collagen gel in aqueous acetic buffer solution (pH 3.5), isolated from horse tendon, was purchased from OPOCRIN SpA, Italy. One weight percent of collagen gel was dissolved in milli-Q water and the assembling of collagen fibers was achieved by increasing the pH up to 5.5 (isoelectric point of collagen) with slow addition of 0.1 M NaOH in aqueous solution (Sigma–Aldrich) [38]. The BDDGE (Sigma–Aldrich) was selected as biocompatible crosslinker to treat collagen fibers and crosslinked collagen fibers were freeze-dried to achieve a porous matrix. By changing the crosslinker percentage and the freeze-drying setup, four different 3D thymus-like collagen constructs were developed and tested. Collagen scaffolds—3% BDDGE with (Coll3_1C) or without a cortical layer (Coll3_WC) were prepared as follows: 150 g of purified collagen fibers were mixed with 45 ml of 1 g/l of BDDGE solution. To efficiently crosslink the collagen fibers, the reaction was performed for 24 hours at room temperature (RT), followed by 24 hours at 4°C. The crosslinking solution was removed by sieving (mesh: 150 µm) and collagen fibers were washed with milli-Q water before pouring them into a polystyrene 48-well

plate [39, 40]. By freezing the collagen hydrogel at −40°C and drying it at 25°C (5 Pa, LIO 3000 PLT, Italy) for 48 hours under a constant vacuum of 0.086 mbar, a porous 3D construct without cortical layer was obtained. For Coll3_WC, collagen fibers were laid out on Mylar sheet and freeze-dried by freezing at −40°C and drying at 25°C (5 Pa, LIO 3000 PLT, Italy) for 48 hours under a constant vacuum of 0.086 mbar. This procedure allows the formation of a single cortical layer at the upper part of the 3D constructs.

Collagen scaffold-BDDGE 5% with one cortical (Coll5_1C) was obtained by adding 150 g of purified collagen fibers to 75 ml of 1 g/l of BDDGE. For the formation of one cortical layer, collagen fibers were treated as previously described for Coll3_WC. Collagen scaffold-BDDGE 3% with two cortical (Coll3_2C) were synthetized using the same procedure described for Coll3_1C. To achieve the second cortical layer, the scaffold was rewet and added with a layer of collagen fibers at the bottom part of the scaffold. Finally, a second freeze-drying cycle, with the same setup described above, was carried out keeping the previous cortical layer in contact with the freezing plate and the new-layered collagen at the upper part.

The morphological microarchitecture of the scaffolds was evaluated by scanning electron microscopy (SEM) performed on specimens mounted onto aluminum stubs using black carbon tapes and sputter coated with gold (Sputter Coater Q150TES, Quorum, Italy). The specimen surface was examined using high resolution SEM (FEI, Quanta 200, U.K.) at a pressure of 0.1 mTorr at an accelerating voltage of 7 or 10 kV. Percentage of porosity was measured by gravimetric method conferring total porosity of the scaffold and by water squeezing method resulting in percentage of macropore volume [41]. The density method measures the scaffold density with weight and volume of dried scaffold; and from the scaffold density, the porosity is calculated as already described in other papers [33, 42, 43]. Porosity values were expressed as the mean $\pm$ SE and the number of replicates ($n$) was three ($n$ = 3). The water squeezing method measures the amount of water inside a scaffold before and after scaffold squeezing. The method is based on the principle that the water is present in small and big pores inside the polymer network [33, 41]. The values were expressed as mean $\pm$ SE ($n$ = 3). Perfusion tests were performed in a U-CUP bioreactor (Cellec, Switzerland). Briefly, the samples were placed in the bioreactor chamber and 12 ml of methylene blue (0.000015 wt/wt %) were added to the column, following the manufacturer's instructions. The liquid flow was set to a constant speed of 3 ml/minute for 24 hours.

### Scaffolds Seeding and In vivo Engraftment

In the experiments showed in the present article, $2 \times 10^5$ TECs were cultured in scaffolds, unless otherwise stated. For in vivo experiments, mice were anesthetized by injecting intraperitoneally 0.5 ml of avertin 240 mg/kg (Sigma–Aldrich) and scaffolds were transplanted subcutaneously (s.c.) in the inguinal area or under the kidney capsule of CD1 athymic nude mice. Wounds were sealed with silk suture (Ethicon) and reinforced by metal clips (CellPoint Scientific, Gaithersburg, MD).

### Flow Cytometric Analyses

To check TEC enrichment after isolation, cells were incubated with anti-CD45 (clone 30-F11, BioLegend, San Diego, CA), anti-EpCam (clone G8.8, BioLegend), anti-Ly5.1 (clone 6C3,

Miltenyi), anti-Ulex Europeaus agglutinin I (clone FL-1061, Vector Laboratories, Burlingame, CA), and anti-Major Histocompatibility Complex (MHC) class II (clone M5/114.15.2, BioLegend) antibodies. Exclusion of dead cells was done adding 200 µg/ml of DAPI solution just before acquisition.

For the evaluation of epithelial stem-progenitor markers, cells were incubated with anti-Epcam (clone G8.8, BioLegend), anti-OCT4 (clone EM92, Ebioscience), anti-CD44 (clone IM7, BD, Biosciences, San Jose, CA), anti-Sca-1 (clone D7, BioLegend), anti-CD90 (clone 30 H-12, BioLegend), and anti-MHC II (clone M5/114.15.2, BioLegend) antibodies.

At the time of sacrifice, mice were euthanized according to the ethical guidelines. Spleen, lymph nodes, and blood samples were prepared using standard protocols and analyzed with anti-CD45 (clone 30-F11, BioLegend), anti-CD3 (clone 145-2C11, BD, Biosciences), anti-CD4 (clone RM4-5, BD, Biosciences), and anti-CD8 (clone 53–6.7, BD, Biosciences) antibodies.

Cells were acquired on a FACS-Canto II or LSR Fortessa flow cytometer (BD, Biosciences) and analyses were performed using the FlowJo software (FlowJo, LLC, Ashland, OR).

## Histology

For immunofluorescence analyses, untransduced or transduced TECs were detached with trypsin EDTA (Lonza) plated on 0.1% gelatin type B (Sigma–Aldrich) precoated glass slides and cultured in X-VIVO10 medium supplemented with the ROCK inhibitor until staining. Cells fixation was performed with 4% paraformaldehyde (Sigma–Aldrich), 15 minutes at RT. Cells were then washed with Dulbecco's phosphate-buffered saline 1× (Corning, NY), permeabilized with 0.3% Triton X-100 (VWR, BDH Chemicals, Radnor, PA) solution for 5 minutes at RT, and incubated with a blocking solution of 5% FBS 1 hour at RT. Primary and secondary antibody incubation was performed in PBS 1× with 5% FBS. Cells were stained with rabbit polyclonal anti-OCT4 primary antibody (clone ab18976, Abcam, U.K.) overnight at 4°C and with Alexa Fluor 647 donkey anti-rabbit secondary antibody (ThermoFisher Scientific, Waltham, MA), 1 hour at RT in the dark. To perform nuclear staining, 200 µg/ml of DAPI solution were added for 5′ at RT in the dark, before mounting the glass slides with Vectashield reagent (Vector Laboratories). Immunofluorescence analyses on in vitro thymic scaffold were performed with the same standard protocol. Images and movies were acquired at San Raffaele Hospital Alembic facility with the Confocal Leica TCS SP2 (Leica Microsystems, Germany).

For immunocytochemistry analyses, mouse scaffold samples were fixed in formalin 4%, paraffin-embedded and, for each sample, five levels were cut on average. Sections of 1.5 µm were used for hematoxylin and eosin (H&E) staining to check for basic histopathological changes. Sections were de-waxed, rehydrated, and endogenous peroxidase activity blocked with 0.1% $H_2O_2$ for 15 minutes. Nonspecific background was reduced with Rodent Block (Biocare Medical, Pacheco, CA) before microwave antigen-retrieval treatment and then slides were incubated with primary antibodies. The following primary antibodies were used: rabbit anti-CD3 (clone SP7; 1:100; ThermoFisher Scientific; EDTA buffer pH 8.0), rabbit anti-cytokeratin 5 (CK5, clone AF 138, 1:100, Covance; EDTA buffer pH 8.0), rat anti-cytokeratin 8 (CK8, clone TROMA-I, 1:200, Developmental Studies Hybridoma Bank, EDTA buffer pH 8.0), anti-myeloperoxidase (MPO) antibody (1:300, Abcam, EDTA buffer pH 8.0), rat anti-F4/80 (1:100,

Bio-Rad, Hercules, CA, DIVA Decloaker 1× Biocare Medical), and goat anti-CD31 (1:1,000; R&D Systems, Minneapolis, MN; DIVA Decloaker 1× Biocare Medical). As secondary antibodies, we used: goat-on-mouse HRP-polymer (Biocare Medical), MACH 1 Universal HRP Polymer Kit (Biocare Medical), or rat-on-mouse HRP-polymer (Biocare Medical) and reactions were developed in Biocare's Betazoid 3,3'-Diaminobenzidine and nuclei counterstained with hematoxylin (Dako, Denmark). Digital images were acquired by an Olympus XC50 camera mounted on a BX51 microscope (Olympus, Japan) with CellF Imaging software (Soft Imaging System GmbH, Germany). Olympus slide scanner VS120-L100 was used to acquire images of the entire sections with H&E staining.

## RT-PCR

TEC RNA was extracted using the RNeasy Micro Kit (QIAGEN, Germany). RNA was stored at −80°C until use. Reverse transcription of mRNA was performed with the High Capacity Reverse Transcription Kit (Applied Biosystems). Real-time PCR for Oct4, Foxn1, and Dll4 was performed with Fast SYBR Green Master Mix (Applied Biosystems) using the Viia-7 Real-Time PCR machine (Applied Biosystems). The following primers were used: GAPDH (5′-ACGGCAAATTCAACGGCACAG-3′ fwd, 5′-ACACCAGTA GACTCCACGACATAC-3′ rev); Oct4 (5′-ACATCGCCAATCAGCTTGG-3′ fwd, 5′-AGAACCATACTCGAACCACATCC-3′ rev); Foxn1 (5′-CTCGTCGTTTGTGCCTGAC-3′ fwd, 5′-TGCCTCTTGTAGGGGTGGAA A-3′ rev); and Dll4 (5′-AGGTGCCACTTCGGTTACAC-3′ fwd, 5′-GGGAGAGCAAATGGCTGATA-3′ rev). For Dll1, AIRE, and PSMB11 RT-PCR was performed using TaqMan Gene expression Assays (Applied Biosystems) and the EagleTaq Universal Master Mix (Roche). All PCR reactions were performed in MicroAmpOptical 96-well reaction plates (Applied Biosystems) in a final volume of 20 µl and run on the Viia-7 Real-Time PCR machine (Applied Biosystems). Relative quantification of genes was performed with the 2−ΔΔCt method, normalized to GAPDH and expressed as fold change relative to the untransduced sample used as control.

## In Vivo Bioluminescence Images Acquisition

Small animal bioluminescence imaging (BLI) was performed by using the IVIS SpectrumCT System (Perkin Elmer, Waltham, MA). The system is composed of a low noise, back-thinned, back-illuminated Charge-Coupled Device camera cooled at −90°C with a quantum efficiency in the visible range above 85%. Each mouse received an intraperitoneal injection of 150 mg luciferin per kilogram body weight 10 minutes before BLI. During image acquisition, the animals were kept at 37°C and under gaseous anesthesia (2%–3% isoflurane and 1 l/minute oxygen). Dynamic BLI was performed by acquiring a set of images every 2 minutes from 10 to 20 minutes after luciferin injection to detect the highest BLI signal. The images were obtained using the following IVIS SpectrumCT System settings: exposure time = auto, binning = 8, $f$ = 1, and a field of view equal to 13 cm (field C). No emission filters were used during BLI acquisitions. BLI image analysis was performed by placing a region of interest (ROI) over the leg and by measuring the total flux (photons/seconds) within the ROI. Images were acquired and analyzed using Living Image 4.5 (Perkin Elmer).

## Ultrasound Imaging

Acquisition was performed using high performance ultrasonographic equipment (Vevo 2100; Fujifilm VisualSonics, Inc., Canada). Anesthetized mice (isoflurane, Isoba; 4% in oxygen for induction, 2% for maintenance at a rate of 1 l/minute) were positioned in a prone position on a heated imaging platform (THM150 MousePad part of the VisualSonics Vevo Integrated Rail System III) and legs taped to electrocardiograph leads to monitor heart and respiration rates. Body temperature was monitored with a rectal probe and maintained at $36.5°C \pm 0.5°C$. A prewarmed ultrasound gel (Aquasonic) was used as a coupling agent between the ultrasound probe and the skin. Two-dimensional (2D) ultrasound images in B-mode (brightness mode) and power Doppler mode were performed using a high-frequency linear array transducer (MicroScan MS 550D; 22–55 MHz; Fujifilm VisualSonics, Inc.) fixed on a railing system. Vascularization of thymic scaffolds was assessed measuring the fractional moving blood volume (FMBV) on a 2D central scan of the implanted structure, where FMBV represents the percentage of moving blood in a ROI drawn along the perimeter of each scaffold.

## Contrast Enhancement Ultrasound

Studies were performed in contrast mode using the MS 250 linear transducer (13–24 MHz; Fujifilm VisualSonics, Inc.). Before contrast enhancement ultrasound (CEUS) imaging, the tail vein was catheterized using a 27-gauge and a PE 20 tubing (2Biological Instruments, Italia). Experiments were performed using MicroMarker untargeted ultrasound contrast agent (CA; Bracco, Switzerland; Fujifilm VisualSonics, Inc.), which consists of gas-filled (nitrogen and perfluorobutane gas) microbubbles (MB; from 0.5 to 5 μm diameter) according to manufacturer's instructions. The reconstituted MB were further diluted to a final concentration of $7 \times 10^8$ MB per milliliter. A total volume of 110 μl of MB suspension was injected in 6 seconds. Sonographic data acquisition started immediately after CA injection and 50 seconds cine loops of contrast wash-in were acquired. Imaging parameters were held constant throughout each experiment to reduce interstudy variability: transmit power 4%; dynamic range 40 dB; center frequency 18 MHz; frame rate 20 Hz; contrast gain 44 dB; gate 4; and beam-width standard. Recorded cine loops were processed for time–intensity curve analysis using the VevoCQ Advanced Contrast Quantification Software (Fujifilm VisualSonics, Inc.). A ROI was drawn along the perimeter of each scaffold. A mathematical equation model based on lognormal distribution function was used to fit the TICs [44]. The peak enhancement (PE) was extracted from the fitted model.

## Magnetic Resonance Imaging

All magnetic resonance imaging (MRI) studies were performed on a 7 T preclinical scanner (Bruker, BioSpec 70/30 USR, Paravision 5.1). All mice underwent imaging under inhalational anesthesia (Isoflurane, 3% for induction and 2% for maintenance in 2 l/minute oxygen) laying prone on a dedicated temperature control apparatus to prevent hypothermia, having breathing rate and body temperature continuously monitored (SA Instruments, Inc., Stony Brook, NY). All mice were prepared to MRI with intravenous injection of gadobutrol (Gadovist; Bayer Schering Pharma, Germany) at a dose of 0.05 μmol/g of body weight. MRI protocol included: rapid acquisition with relaxation enhancement (RARE) T1-weighted sequence, RARE with variable repetition time TR (RAREVTR) sequence for quantitative T1 relaxation maps, and Fast Low Angle SHot (FLASH) sequence for dynamic contrast-enhanced. The sequences were acquired in the axial plane; the thickness of slice axial sections was 1 mm without spacing slice of contiguous images.

## Statistical Analyses

All data sets were analyzed using GraphPad Prism software and expressed as median and SD. Statistical significance was assessed using nonparametric one-way analysis of variance Kruskal–Wallis test with Dunn's multiple comparison. NS, $p > .05$; *, $p \leq .05$; **, $p \leq .01$; ***, $p \leq .001$; ****, $p \leq .0001$. $p$ values <.05 were considered significant.

### RESULTS

### Generation of Collagen-Based Scaffolds Mimicking the Thymic Ultrastructure

Four different collagen-based scaffolds were developed in order to create a 3D ultrastructure closely reproducing the murine thymus morphology [45–47]. Self-assembled collagen fibers present typically poor mechanical properties and rapid in vivo enzymatic degradation. To overcome these limitations, a crosslinking reaction was performed using BDDGE. BDDGE, a symmetric di-epoxide molecule was selected due to its well-known biocompatibility at low concentration and its ability to react selectively with aminic and/or carboxylic functions of collagen molecules depending on the pH of the reaction environment [48]. The crosslinking reaction was performed at 25°C and pH 5.5 to obtain a good compromise between molecular assembling and chemical crosslinking. In these conditions, BDDGE created bridges between collagen fibers improving the mechanical performance and decreasing the enzymatic degradation [39]. By changing the crosslinker concentration and the fibers freeze-drying technique, four different collagen-based scaffolds were developed (Fig. 1A). The scaffold Coll3_WC was synthetized without the cortical layer and showed a homogeneous porosity in the upper part, resembling the medullary region of the thymus. This morphology led to a highly open porous-structure and consequently permitted a good perfusion of the scaffold when tested in dynamic conditions using the bioreactor. However, Coll3_WC did not completely recapitulate the thymic morphology, since it was lacking a cortical-like region, and was, therefore, not further considered for in vitro and in vivo experiments. We further tested samples Coll3_1C and Coll5_1C, which contained both a collagen fibers organization similar to the medulla ECM and a denser pattern suggestive of the cortex. Both samples were characterized by high porosity as demonstrated by density and water squeezing methods (Fig. 1A) very similar to those observed for Coll3_WC. The higher crosslinking strength used for sample Coll5_1C induced the formation of a thicker cortical layer, precluding an efficacious perfusion of the scaffold. An additional collagen-based scaffold was successfully developed (Coll3_2C) adding a second cortical layer while keeping the medulla like structure in the scaffold's center, which created an ultrastructure as in a native thymus. The presence of a double cortical layer slightly decreased the porosity of this type of scaffold and completely prevented its perfusion when the bioreactor perfusion-test was performed. Therefore, Coll3_2C was not taken into consideration for further experiments. Figure 1B shows SEM images of a murine native
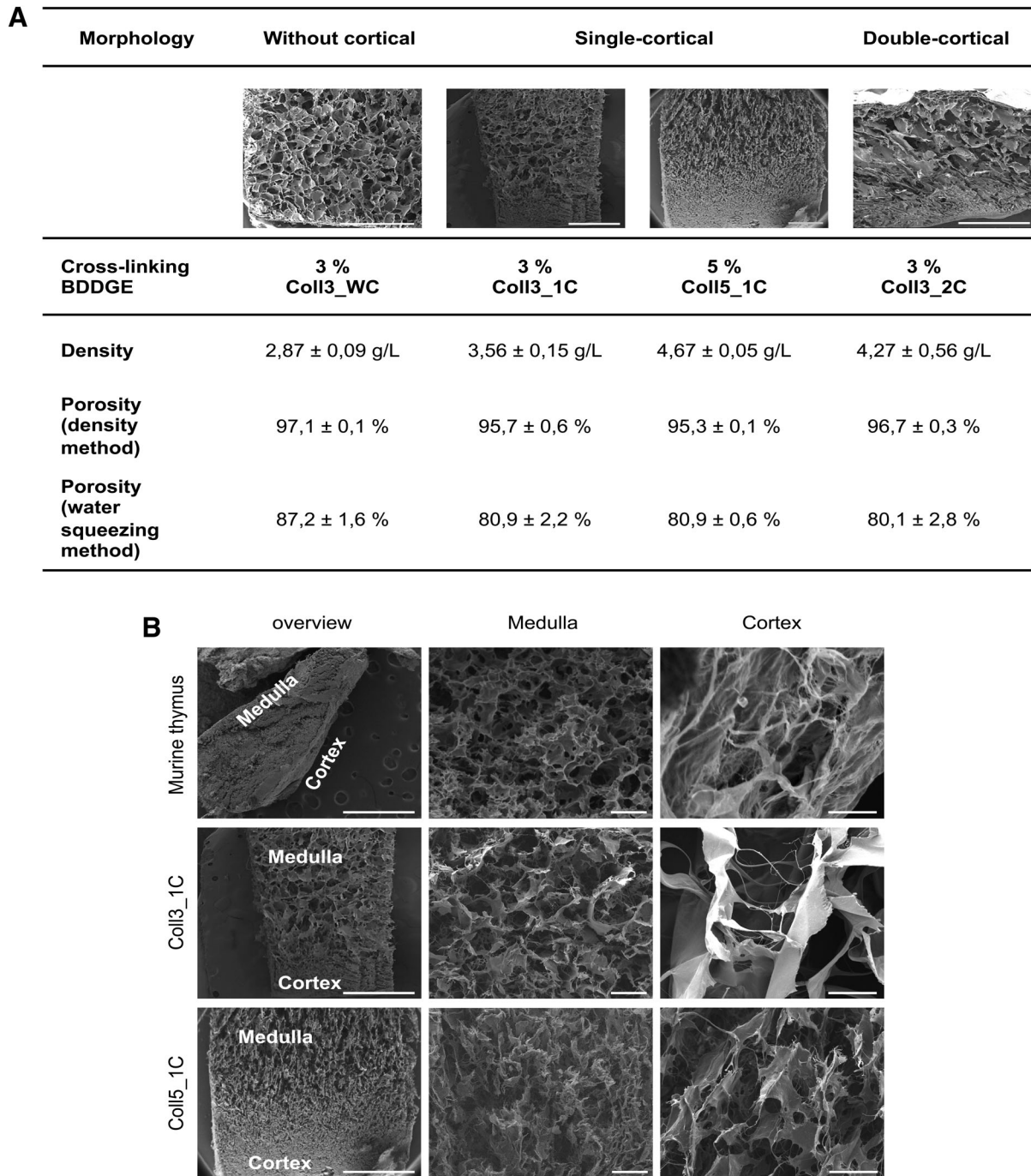
**A**



| Morphology | Without cortical | Single-cortical | | Double-cortical |
|---|---|---|---|---|
| **Cross-linking BDDGE** | **3 %** **Coll3_WC** | **3 %** **Coll3_1C** | **5 %** **Coll5_1C** | **3 %** **Coll3_2C** |
| **Density** | 2,87 ± 0,09 g/L | 3,56 ± 0,15 g/L | 4,67 ± 0,05 g/L | 4,27 ± 0,56 g/L |
| **Porosity (density method)** | 97,1 ± 0,1 % | 95,7 ± 0,6 % | 95,3 ± 0,1 % | 96,7 ± 0,3 % |
| **Porosity (water squeezing method)** | 87,2 ± 1,6 % | 80,9 ± 2,2 % | 80,9 ± 0,6 % | 80,1 ± 2,8 % |

**B**



**Figure 1.** Generation of collagen-based scaffolds mimicking the thymic ultrastructure. **(A):** 3% and 5% 1,4-butanediol diglycidyl ether (BDDGE) collagen type I scaffolds with different structures were tested to check their porosity, density, and perfusion ability. Scaffold dimension: 8 mm × 8 mm × 4 mm. **(B):** Electron microscopy images showing the ultrastructure of a murine native thymus and collagen type I scaffolds with two different percentages, 3% (Coll3_1C) and 5% (Coll5_1C), of the crosslinker BDDGE and one cortical layer. Our scaffolds recapitulate the medullary and cortical features of a normal thymus. Scale bar: 200 µm for medulla and cortex magnification; 10 mm for overview magnification.

thymus and of samples Coll3_1C and Coll5_1C. This comparison revealed their similar morphology to native thymic tissue indicating a good biomimicry of the selected scaffolds. Even though the higher amount of BDDGE (5%) led to an increase of thickness of the cortical layer in scaffold Coll5_1C, we considered both Coll3_1C and Coll5_1C appropriate for further experiments.

### Inducible Expression of Oct4 in Adult TECs Results in Transient Expression of Progenitor Markers and Improves Its In Vitro Proliferation

We isolated primary adult TECs from 4 to 6 weeks old WT mice (C57BL/6) by enzymatic digestion followed by CD45+ cell-depletion. After depletion, TEC enrichment was evaluated by

flow cytometry based on the frequency of Epcam+ cells and ranged from 15% to 30% in all experiments performed. To promote TEC in vitro expansion and proliferation, we developed a tetracycline-regulated Oct4 expression system, consisting of two LVs: a bi-directional regulator vector that stably expressed the Tet-On transactivator protein (rtTA) and the mCherry fluorescent protein, and a response vector driving the expression of the human *Oct4* coding sequence and the vexGFP marker under the control of a tetracycline-inducible promoter (referred to as the Oct4.vexGFP; Fig. 2A).

As proven by immunofluorescence analyses, cells transduced with both vectors and kept in culture in the presence of doxycycline (iOCT4 doxy or iOCT4 TECs) expressed both mCherry and Oct4.vexGFP. On the other hand, TECs transduced with both vectors but cultured in the absence of doxycycline (iOct4 no doxy) expressed mCherry but not Oct4 nor vexGFP (Fig. 2B). Additionally, the expression level of Oct4 was increased in iOct4 doxy samples as compared with the basal expression level observed in freshly isolated TECs (Supporting Information Fig. S1) or in UT or PGK.GFP transduced TECs (Fig. 2D). Oct4 expression, as verified both by flow cytometric analyses (Fig. 2C, upper panel) and by immunofluorescence (Fig. 2C, lower panel), was drastically reduced in 5 days (iOCT4 TECs doxy without d5) and completely absent 7 days after doxycycline removal from the culture medium (iOCT4 TECs doxy without d7), confirming the strength and reversibility of the LV system in controlling Oct4 expression upon transduction. Inducible expression of Oct4 induced only a partial de-differentiation of TECs, as proven by phenotypical comparison between iOCT4 TECs and UT TECs (Fig. 2D). Indeed, Oct4 upmodulation led to an increase in the expression levels of precursor-like markers (Thy1.2+/Sca1hi) [49, 50] and a more homogeneous expression of MHC II, an important molecule for TEC functionality. Of note, iOCT4 TECs maintained their epithelial phenotype, as shown by the expression of molecules associated with TECs differentiation (CD44) and with TECs specification (Epcam). Doxycycline washout from the culture reverted iOCT4 TEC phenotype, since 5 days after its removal (doxy without d5) iOCT4 TECs showed a phenotype similar to UT TECs (Fig. 2D). RT-PCR analyses demonstrated that Oct4 mRNA levels, relative to UT, were increased more than 100-fold in iOCT4 TECs even after 1 passage in vitro and returned at basal levels upon doxycycline removal (Fig. 2E). Importantly, upmodulation of Oct4 in TECs strongly improved their in vitro expansion over time. Indeed, iOCT4 TECs showed a twofold increase in proliferation rate as compared with untransduced TECs, indicating that Oct4 is a good candidate for promoting in vitro expansion of postnatal TECs (Fig. 2F). Moreover, the mRNA levels of Foxn1, AIRE, PSMB11, and Dll1, fundamental genes for TEC growth, differentiation, and function, did not change after transduction or upon Oct4 down-regulation. On the other hand, Dll4 expression, a Foxn1-target gene, which is critical for the commitment of lymphoid precursors to a T-cell fate [51], increased when iOCT4 TEC differentiation was induced after doxycycline washout (Supporting Information Fig. S2).

### 3% BDDGE Collagen Type I Scaffolds Are More Efficient for iOCT4 TECs Expansion and the Formation of Vascular Structures After In Vivo Transplantation in Athymic Nude Mice

In order to use postnatal TECs for the generation of transplantable thymic-like structures, we exploited the 3D collagen type I scaffolds with different BDDGE crosslinking strength as previously described (Fig. 1). UT TECs or iOCT4 TECs were seeded in 3% or 5% BDDGE scaffolds between day 10 and 13 after 2D culture and kept in culture at 37°C in X-VIVO10 medium, in the presence of the ROCK inhibitor, with or without doxycycline. At different time points after TEC seeding, 3D collagen scaffolds were visualized using confocal microscopy demonstrating that the 3D structure allowed the survival and expansion of iOCT4 TECs up to 30 days after isolation (Supporting Information Fig. S3).

For in vivo experiments, thymic scaffolds were kept in culture for less than 5 days after TEC seeding in the 3D structure and were then transplanted subcutaneously in the back or inguinal area of CD1 BALB/c nude mice. Ultrasound analyses of transplanted scaffolds were performed to detect and quantify vascular structures, which are needed for nutrients supply into the organoid. We observed that 3% BDDGE scaffolds were better vascularized than 5% BDDGE scaffolds and this was evident both for UT and for iOCT4 TEC-seeded structures (Fig. 3A). These results were also confirmed by CEUS analyses (Fig. 3B) of the same mice shown in panel (A), which were transplanted with 3% UT TECs (upper panel) or with iOCT4 TECs-seeded (lower panel) scaffolds. Of note, images acquired 2 weeks after grafting revealed the presence of a constant vascularization only inside the iOCT4 TEC-seeded structures (lower panel). MRI of a mouse transplanted with 3% BDDGE scaffold seeded with iOCT4 TECs performed 2 weeks after transplantation confirmed persistent perfusion of the 3D construct, demonstrated by the gadolinium-related enhancement (Fig. 3C, white arrows). By immunohistochemistry, higher numbers of CD31+ endothelial cells were detected in the central areas of the iOCT4 TECs seeded scaffold as compared with empty scaffolds or to those seeded with UT or no doxy iOct4 TECs (Fig. 3D, 3E).

Since 3% BDDGE collagen type I scaffolds showed a better performance than 5% BDDGE scaffolds, we decided to use this type of 3D structure for further investigations. To attest the in vivo persistence of 3% BDDGE scaffolds, the 3D structures were transplanted in athymic nude mice and analyzed with the IVIS SpectrumCT in vivo imaging system. Each transplanted scaffold was obtained by seeding TEC UT or transduced with PGK.GFP LV or with the Oct4-inducible LV system. For these experiments, we used a bi-directional regulator vector that stably expressed the Tet-On trans-activator protein (rtTA) and the firefly-luciferase gene (Fig. 2A). BLI of transplanted animals was obtained by injecting luciferin 1 week (Fig. 4A, upper panel) or 2 weeks (Fig. 4A, lower panel) after transplantation. Luciferase signal was clearly visible in mice transplanted with iOCT4 TEC-seeded scaffolds (mice 4, 5, 6, 7) 1 week after implantation but dropped 1 week after and was completely absent at both time points in control mice (Supporting Information Table S1 shows ROI values for each mouse at each time point of analysis). Mice number 5 and 6, transplanted with iOCT4 TECs-seeded scaffolds, showed in vivo persistency of iOCT4 TECs within the scaffold (Fig. 4B). With these analyses, we confirmed the in vivo persistence of iOCT4 TECs inside the scaffold even though the fluorescence intensity and the number of live iOCT4 TECs were likely reduced 2 weeks after scaffold implantation. Interestingly, immunohistochemical analyses of tissue sections from grafted scaffolds seeded with either UT TECs or with iOCT4 TECs, exposed or not to doxycycline, demonstrated the presence of both cortical (CK8+ cells) and medullary (CK5+ cells) TECs in their inner part. The number of CK5+ and CK8+ cells was most
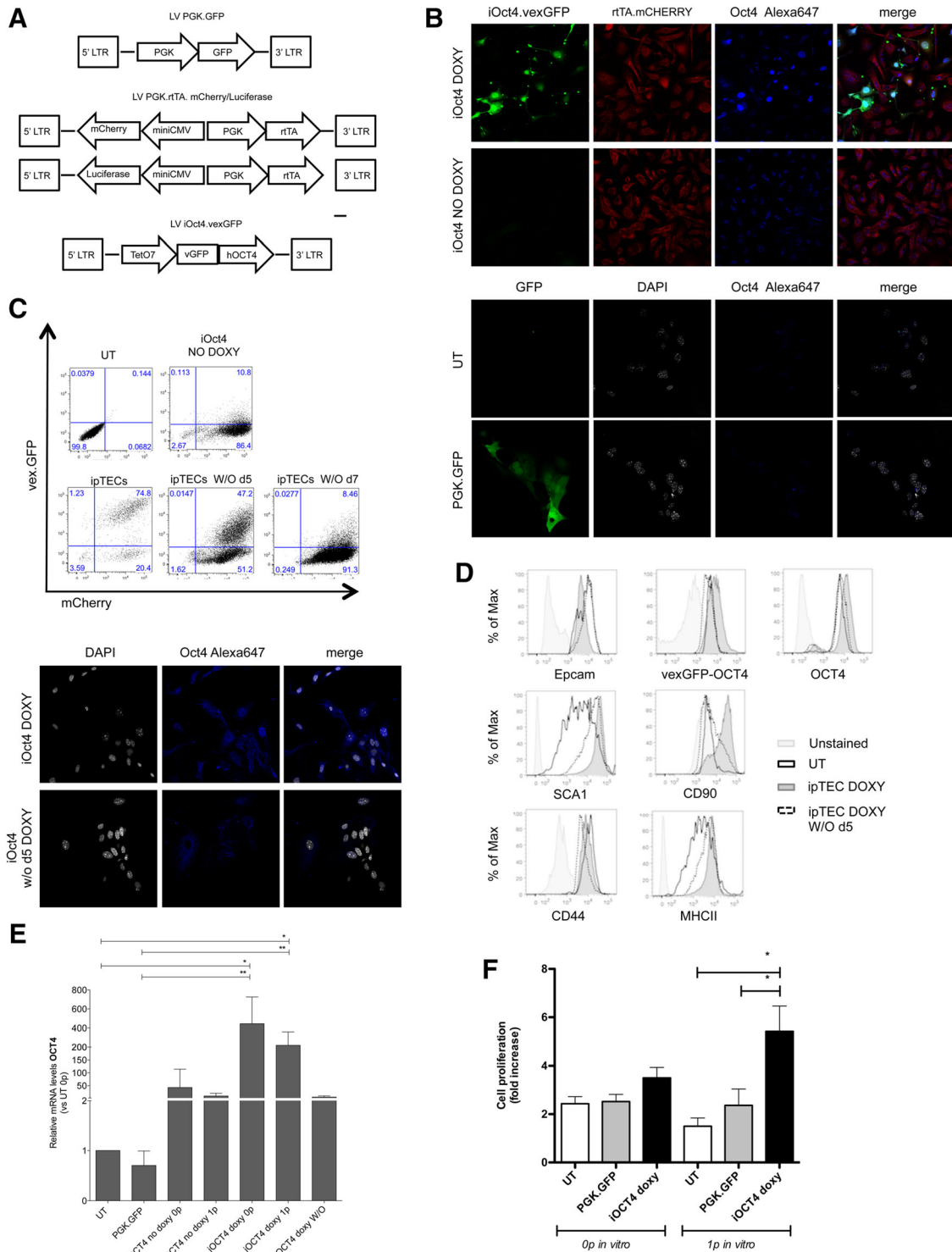
**Figure 2.** Inducible expression of Oct4 in adult thymic epithelial cells (TECs) improves its in vitro proliferation and induces the expression of progenitor markers. **(A):** Maps of the lentiviral vectors (LVs) used in this paper. **(B):** Freshly isolated TEC were transduced with PGK.GFP LV or with LVs for the inducible expression of Oct4 cultured with (iOct4 DOXY) or without doxycycline (iOct4 NO DOXY). Untransduced TEC (UT) was used as control. Oct4 immunofluorescence analyses were performed 7 days after transduction. **(C):** Flow cytometric (upper panel) and immunofluorescence (lower panel) analyses for the expression of OCT4-vex.GFP 5 or 7 days after doxycycline removal from the culture medium (iOCT4 TECs washout d5 and d7, respectively). **(D):** Flow cytometric analyses for the expression of stem-progenitor markers (Thy1.2/CD90, Sca1) and for the expression of molecules important for thymus development and functionality (Epcam, MHC II, and CD44). **(E):** RT-PCR analyses for the expression of Oct4 (one-way analysis of variance [ANOVA] with Dunn's multiple comparison test; $p = .0001$. UT $n = 4$ replicates; PGK.GFP $n = 4$ replicates; iOCT4 no doxy 0p = 5 replicates; iOCT4 no doxy 1p = 3 replicates; iOCT4 doxy 0p = 4 replicates; iOCT4 doxy 1p = 5 replicates; iOCT4 doxy washout = 7 replicates). **(F):** TECs in vitro expansion has been evaluated as fold increase in their proliferation rate. Cultures were counted every 3 days. Fold increase of cells was determined by total cell number recovered divided by the initial cell number plated (one-way ANOVA with Newman–Keuls multiple comparison test. $p = .0791$ and $p = .0042$ for in vitro passage 0 and passage 1, respectively).
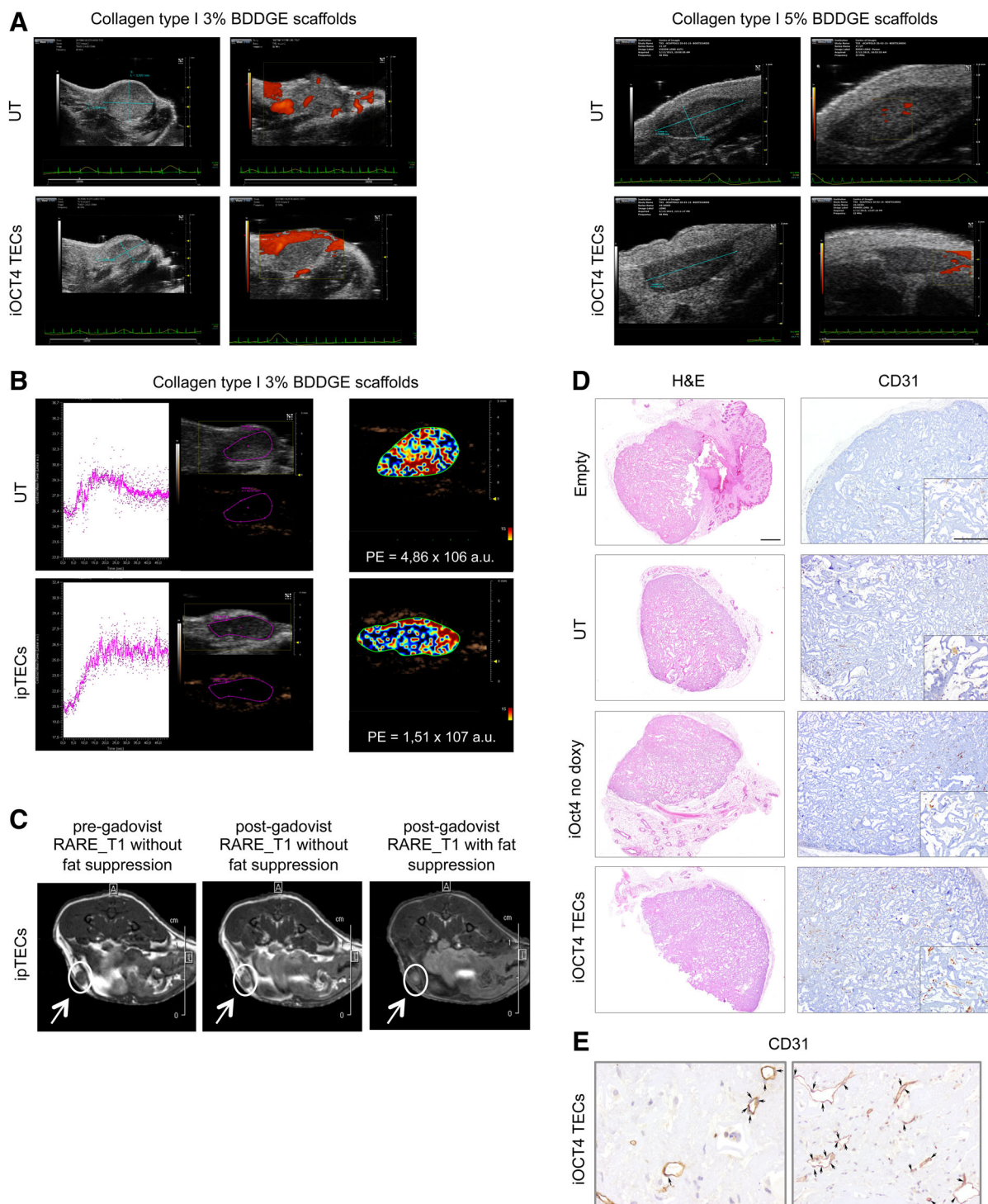
**Figure 3.** 3% 1,4-butanediol diglycidyl ether (BDDGE) collagen type I scaffolds are more efficient in the formation of vascular structures after in vivo transplantation in athymic nude mice. **(A):** Ultrasound image of a mouse transplanted with 3% (left panel) or 5% BDDGE (right panel) scaffolds seeded with untransduced thymic epithelial cell (TEC) or with iOCT4 TECs. Images were acquired 2 weeks after in vivo transplant. Micromarker contrast agent (CA) was injected at time 0 and the uptake of the CA was recorded for 50 seconds. **(B):** Quantitative analysis of 3% BDDGE scaffolds perfusion was performed using Vevo CQ software: the peak enhancement (PE) was calculated for the largest cross-section of each scaffold. Gray-scale image and the nonlinear contrast image of the two scaffolds (left) are displayed with the corresponding color-coded PE parametric map (right). **(C):** Magnetic resonance imaging of a mouse transplanted with 3% BDDGE scaffold seeded with LV iOct4.vexGFP transduced TEC performed 2 weeks after scaffold transplantation, showing, by contrast, the perfusion of the scaffold before and after gadolinium injection (white arrows). **(D):** Scaffold sections, 2 weeks after transplantation, were stained with H&E or CD31 to detect new blood vessel formation. For each group of mice, a central section of the scaffold was chosen for IHC analyses. Scale bar: H&E 500 µm, CD31 500 µm, CD31 inset 200 µm. **(E):** Enlargement (50 µm) of iOCT4 scaffold section stained with CD31 antibody 2 weeks after transplantation. Each cross indicates CD31 positive endothelial cells, allowing a better discrimination for the formation of a primordium of vascular network.
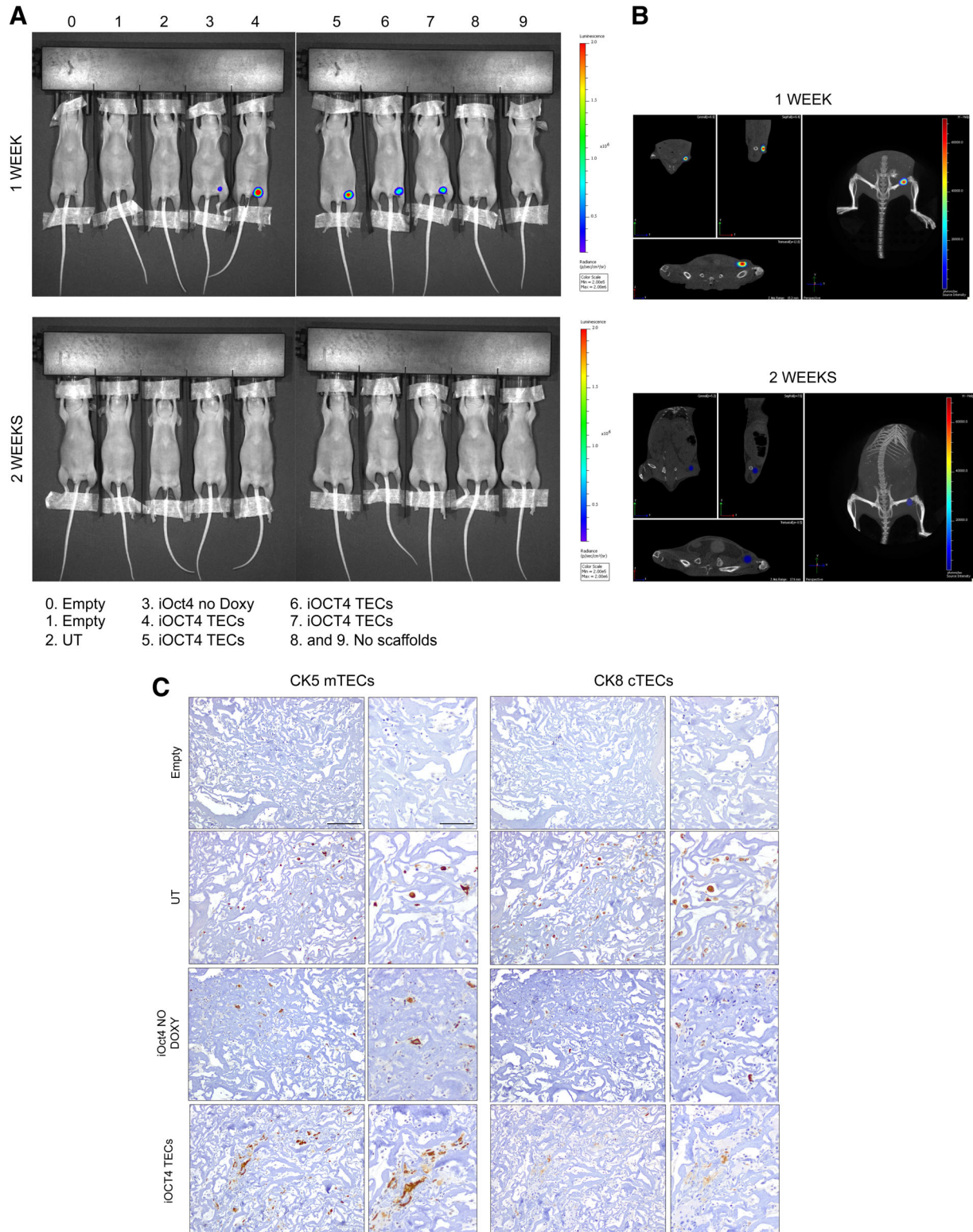
**Figure 4.** 3% 1,4-butanediol diglycidyl ether collagen type I scaffolds are more efficient for iOCT4 thymic epithelial cells (TECs) expansion after in vivo transplantation in athymic nude mice. **(A):** Images of transplanted animals were acquired by IVIS series preclinical in vivo system, 1 week (upper panel) or 2 weeks (lower panel) after scaffolds transplantation. Color scale is reported on the right side of the image. **(B):** Quantitative optical and computed tomography using IVIS series preclinical in vivo imaging system of mouse 5 (upper panel) or mouse 6 (lower panel), 1 week or 2 weeks after transplantation, respectively. Color scale is reported on the right side of the image. **(C):** Immunohistochemistry analyses for detection of CK5+ medullary TECs or CK8+ cortical TECs inside scaffolds of transplanted animals 2 weeks after transplantation in athymic nude mice. Inner and serial sections were chosen for the analysis. Scale bar: 200 μm, 100 μm for magnification on the right panel.

prominent in iOCT4 TECs thymic scaffolds indicating that these cells were able to survive and proliferate better in vivo under the chosen conditions. Strikingly, in iOCT4 TEC-seeded scaffolds, we detected the formation of small clusters formed by few mTECs (CK5+) and cTECs (CK8+), revealing that the 3D structure used in our experiments supports the compartmentalization and proliferation of mature TECs (Fig. 4C).

### Thymic-Like Structures Generated with iOCT4 TECs Do Not Support Clear Thymopoiesis After Implantation in Athymic Nude Mice

We next evaluated whether implanted TEC-seeded 3D structures had the ability to attract T-cell precursors and subsequently allow for their differentiation into T lymphocytes. For this purpose, thymic-like structures were implanted s.c. in athymic nude mice and the presence and maturation of newly formed T lymphocytes were evaluated in the periphery at different time points (4, 6, and 10 weeks) after implantation. We performed immunohistochemistry analyses of 3D thymic-like structures from mice transplanted with 3% BDDGE empty scaffolds or seeded with UT or LV iOCT4-transduced TECs, cultured with or without doxycycline, 2 weeks after transplantation. CD3+ lymphocytes were absent in empty or UT scaffolds, barely detectable in those seeded with iOCT4 no doxy TECs and slightly increased in thymic scaffolds seeded with iOCT4 TECs (Fig. 5A). Unfortunately, flow cytometric analysis could not be performed because of the scarcity of the cells recovered from the scaffolds and immunohistochemistry staining for CD4 and CD8 were not possible in scaffolds, thus preventing us from positively concluding that thymopoiesis was taking place in the iOCT4 TEC-seeded scaffolds. Flow cytometry analyses of peripheral blood (PB) of transplanted animals showed that at the first time point analyzed after transplantation (4 weeks), the frequency of circulating CD45+CD3+ cells in the PB of mice transplanted with iOCT4 TEC-seeded thymic-like structures was higher than in control groups (UT/PGK.GFP and TECs no doxy scaffolds; Fig. 5B). The frequency of CD45+CD3+ cells in the PB of mice transplanted with iOCT4 TECs-containing thymic-like structures kept increasing 6 and 10 weeks after transplantation, but it was not statistically different from the increment observed in control groups (Fig. 5B). In the PB of mice transplanted with iOCT4 TEC-seeded 3D thymic-like structures, CD45+CD3+CD4+ and CD45+CD3+CD8+ cells were present, and their frequency improved over time (Fig. 5C).

Increased proportions of activated/memory CD4+ T cells were evident in iOCT4 TEC-transplanted mice, which suggest lymphopenia-induced homeostatic expansion of newly generated T cells (Supporting Information Fig. S4) [52]. At sacrifice, we did not detect significant differences in proportion and absolute counts of CD4+ and CD8+ T cells in spleen and lymph nodes among the different experimental groups (Supporting Information Fig. S5).

### 3% BDDGE Collagen Type I Scaffold Is Degraded 2 Weeks After In Vivo Transplantation

Our results clearly show that the 3% BDDGE scaffold formulation could efficiently support iOCT4 TEC growth, survival, and function in a 3D environment and after in vivo transplantation. However, the luciferase signal dropped 2 weeks after in vivo implantation, suggesting that the 3D thymic-like structure was damaged or completely lost (Fig. 4A). Indeed, iOCT4 TEC-seeded thymic-like structures were able to support T-cell differentiation up to 4 weeks after implantation, but this capability was drastically reduced or lost afterward.

To check the integrity of the thymic-like structures over the course of the first 2 and 4 weeks, MPO and F4/80 staining were performed on grafts. Immunostaining clearly indicated that, already at 2 weeks after transplantation, neutrophils and macrophages colonize thymic scaffolds, irrespective of the type of cells used initially to seed the scaffolds (Fig. 6A). Moreover, the H&E staining showed that phagocytes invaded the scaffold from the derma just above the site of transplantation. We hypothesize that innate immune cells induce a very quick degradation of scaffolds' ECM in vivo, compromising the ability of the 3D structure to support TEC growth and functionality and consequent thymopoiesis (Fig. 6).

## DISCUSSION

In the last decade, several efforts have been made to improve tissue-engineering methods to create artificial thymic organoids or to grow thymic tissue ex vivo [19, 20].

In the search for the most suitable biomaterial to generate transplantable 3D thymic structures, we selected collagen. Indeed, collagen can be easily isolated from animal connective tissues and it has been widely used in tissue engineering, because it is biocompatible, biodegradable, and bioresorbable. It can be simply assembled in fibers closely reproducing the chemical, physical, and morphological characteristics of those present in soft tissues [32, 33]. The 3D scaffolds that we developed have been formulated by modifying type I collagen matrix with different crosslinking approaches to reduce scaffold degradation rate when transplanted in vivo. The 3% BDDGE crosslinker concentration has been finally chosen over the 5% concentration as it conferred to the 3D scaffold a level of porosity, which is indispensable for its performance, which resembled the one typical native thymic ultrastructure. Indeed, scaffolds should have a well-connected porous structure and a high porosity to ensure cellular penetration, nutrients diffusion, and waste products removal in order to decrease any interference between the scaffold and surrounding tissues [53]. To this scope, we firstly analyzed the ultrastructure of a juvenile murine thymus and optimized the protocol for creating scaffolds that would be characterized by a porous part, similar to the thymic medulla, and a fibrous part recapitulating the thymic cortex. Particularly, the vertical and controlled freezing allowed the creation of an aligned highly porous structure at one side and a less porous but hardier surface at the other side of the scaffold (Coll3_1C) [41]. As a consequence, Coll3_1C scaffolds seemed to be the most appropriate among all the scaffolds tested for the creation of thymic organoids, since they combined a well-fitted morphology with a high porosity. Even though the pore size of Coll3_1C scaffolds was bigger than that of the native thymus, this attribute ensured a higher cell penetration and scaffold colonization. By using the 3% BDDGE 3D scaffolds, we could demonstrate that iOCT4 TECs were able to colonize them and to expand in vitro for up to 1 month, whereas untransduced TECs were lost in less than 2 weeks after seeding in the scaffolds. Hence, our approach that combined the use of collagen fibers with the development of a 3D structure met important structural characteristics of the native thymus and reproduced a 3D environment similar to the thymic ECM, perfectly recognized by TECs.
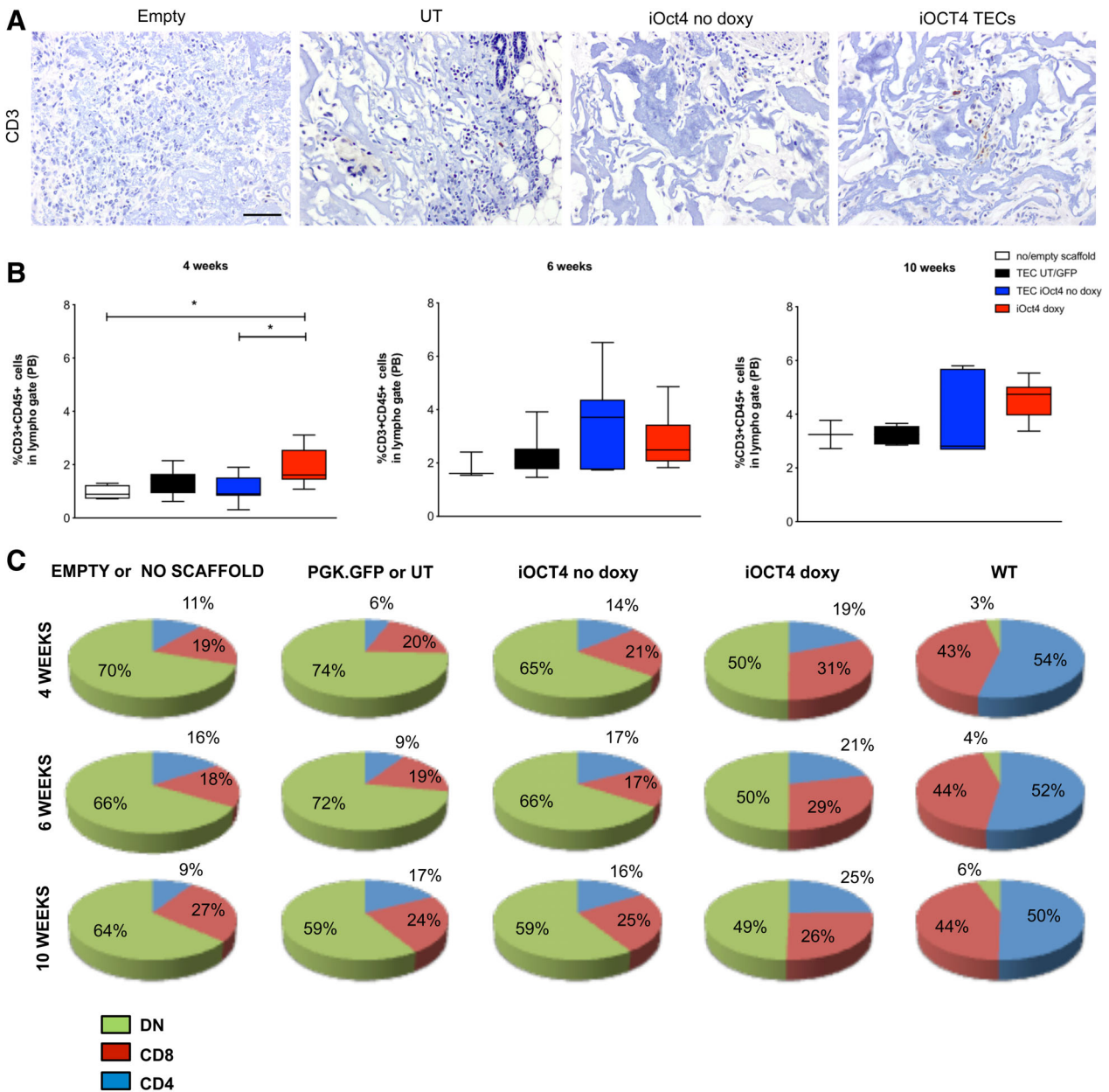
**Figure 5.** Thymic scaffolds generated with iOCT4 thymic epithelial cell (TEC) do not support clear thymopoiesis after implantation in athymic nude mice. **(A):** Two weeks after scaffold transplantation, ex vivo immunohistochemistry analysis of mice transplanted with scaffolds seeded with untransduced TEC (UT) or with lentiviral vector (LV) for Oct4 inducible expression (doxy or no doxy) was performed to detect thymocytes development by CD3 staining. Scale bar: 100 μm. **(B, C):** Peripheral blood analyses of mice transplanted with 3% 1,4-butanediol diglycidyl ether collagen type I scaffolds seeded with 60,000–400,000 of UT, LV PGK.GFP, or with LV iOct4-transduced TEC cultured in the presence or absence of doxycycline at different time points after subcutaneously in vivo transplantation (mean of four experiments). In (B), the graphs summarize the frequency of CD45+CD3+ cells in different groups of animals at indicated time points (one-way analysis of variance with Dunn's multiple comparison test). At 4 weeks: iOCT4 TEC scaffolds $n = 13$; UT/PGK.GFP scaffolds $n = 9$; TECs no doxy scaffolds $n = 9$; empty/no scaffold $n = 4$, $p = .0083$. At 6 weeks: iOCT4 TECs-scaffolds $n = 11$; UT/PGK.GFP scaffolds $n = 7$; TECs no doxy scaffolds $n = 8$; empty/no scaffolds $n = 3$, $p = .1216$. At 10 weeks: iOCT4 TECs-scaffolds $n = 9$; UT/PGK.GFP scaffolds $n = 5$; TECs no doxy scaffolds $n = 5$; empty or no scaffolds $n = 2$, $p = .1854$). In (C), the frequency of CD4+, CD8+, and DN cell of the same groups of animals 4, 6, and 10 weeks after transplantation are reported as pie charts.

In vitro 3D models for the generation of T cells, made with fetal thymic cells (fetal thymic organoids cultures [FTOCs]) [54], demonstrated to partially support the generation of all T-cell subsets. To avoid the use of fetal TECs, as a variant of FTOC, the RTOC (reaggregate thymic organ cultures [RTOCs]) [55] were developed by using adult TECs or adult TEPCs but they failed to support HSC differentiation toward T-cell lineages [26]. Indeed, adult TECs lose their ability to aggregate ex vivo and fail to maintain expression of important molecules, such as those of the Notch signaling pathway, when are not supported by a well-organized 3D environment. Based on this insight, other researchers were able to successfully establish in vitro bone marrow derived cell lines (OP9-DL1 or MS5-Dll4 or MS5-Dll1) or human thymic stromal cell lines (TEC-Dl1) overexpressing the Notch ligand delta-like 1 (Dll1) and Notch ligand delta-like 4 (Dll4) [56, 57]. Even though these experimental systems were able to
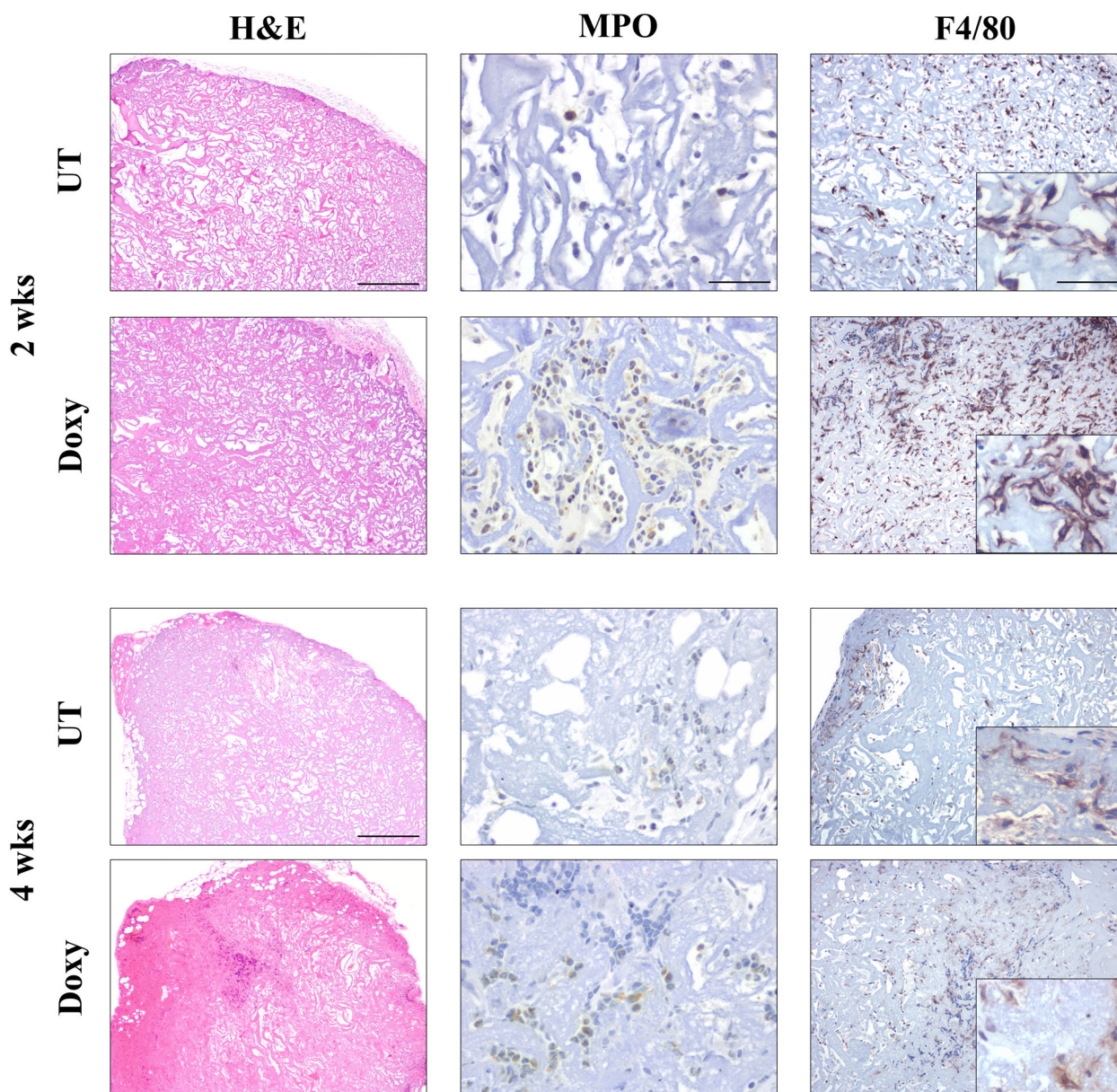
| H&E | MPO | F4/80 |
|-----|-----|-------|



**Figure 6.** 3% 1,4-butanediol diglycidyl ether collagen type I scaffold are degraded starting from 2 weeks after in vivo transplantation. Immunohistochemistry analyses for myeloperoxidase (MPO) and F4/80 detection. Mice were transplanted with scaffolds seeded with untransduced thymic epithelial cell (TEC) or with LV iOct4-transduced TEC, 2 and 4 weeks after scaffold transplantation in athymic nude mice scaffolds were recovered and stained with MPO and F4/80 for neutrophils and macrophages detection, respectively. Inner and serial sections were chosen for the analysis. Scale bar: H&E 500 μm, MPO 50 μm, F4/80 (10×) 200 μm, and the inset 50 μm.

partially support thymocyte development in vitro, they could not recapitulate the complexity of the 3D thymic microenvironment and were not meant to create a functional approach for in vivo thymic regeneration. Our methodologies aimed at accomplishing all these requirements since it combined the use of 3D scaffolds, fully recapitulating the thymic microenvironment, with murine adult derived iOCT4 TECs. By an inducible upmodulation of Oct4 expression, we were able to promote mature TECs in vitro expansion without altering their functionality. Indeed, iOCT4 TECs maintained an epithelial phenotype, since they still expressed Epcam and CD44 after transduction, and most importantly, did not lose the expression of molecules such as Foxn1, AIRE, Dll1, Dll4, and MHC class II, proven to be fundamental for

TEC functionality. However, a deeper expression profile analysis would be necessary in order to fully dissect the molecular mechanism by which Oct4 upmodulation acts in remodeling TEC expression profile and epigenome, since the role of Oct4 in promoting stem-progenitor cells self-renewal during embryogenesis or in inducing pluripotency in somatic cells is well known [34, 58]. Although this point needs further investigation, the induction of Oct4 in our approach is only transient and our results demonstrated that the transient expression of Oct4 did not drastically change the cell lineage identity of adult TECs, since their epithelial phenotype was preserved and most importantly they did not lose the expression of molecules and gene essential for TEC functionality. Additionally, when tetracycline was removed from the

culture medium, iOCT4 TECs reacquired a phenotype very much resembling that of freshly isolated TECs, further confirming that our LV-based system was able to control the expression of Oct4 without radically changing the nature of adult TECs. Importantly, Oct4 expression in adult TECs induced the expansion of a population of cells that presented an improved ability to support T-cell differentiation in vivo, as compared with untransduced TEC or TEC transduced with the iOct4 LV system but not cultured with tetracycline, since thymic scaffolds generated with iOCT4 TEC supported a first wave of thymopoiesis 4 weeks after implantation in athymic nude mice. Indeed, in mice transplanted with 3D iOCT4 TEC structure, CD45+CD3+ cells were clearly visible already at 2 weeks after scaffold implantation and their frequency kept increasing over time, up to 10 weeks after transplant. Even though we detected some CD3+ cells in control groups, their frequency was significantly higher in animals transplanted iOCT4 TEC-seeded scaffolds at the first time point analyzed (4 weeks). Significantly, in the PB of mice implanted with iOCT4 TEC-seeded scaffolds, discrete populations of CD45+CD3+CD4+ and CD45+CD3+CD8+ cells were evident and improved over time. Of note, the frequency of T-cell subsets in the PB of mice transplanted iOCT4 TEC-seeded scaffolds was higher than that observed in other publications using similar approaches for thymus regeneration [22, 59]. In line with previous publications, we found that in all groups of animals, over 50% of circulating CD45+CD3+ cells did not express CD4 or CD8 and they are marked as double negative (DN) CD4−CD8− cells. A slight reduction in the frequency of DN T cells was detected in all transplanted animals [60, 61]. We could not exclude that also in athymic nude mice a residual thymopoiesis may occur over time and this could explain the appearance of SP CD4+ and CD8+ cells also in the PB of mice that were not transplanted with scaffolds. Nonetheless, the increase of the DN and SP cell frequencies observed in these animals was not constant and did not keep increasing over time as conversely observed for mice implanted with iOCT4 TEC-seeded scaffolds. Nevertheless, no major biological effects were achieved in animals transplanted with iOCT4 TEC-seeded scaffolds and no amelioration of the nude phenotype was observed.

The strength of our system resides in the induction of Oct4 expression in TECs, which increases TEC proliferative ability and makes iOCT4 TECs functionally capable of growing in a 3D structure. We provide the first evidence that adult TECs can expand and survive in vitro. Further optimization of the experimental setting exploiting also novel recent biotechnological tools as well as the use of a biomimetic smart scaffold functionalized to decrease immune reactions need to be implemented for the future development of the protocol.

One of the most important features that our 3D thymic structure addressed was their ability to be vascularized in vivo after implantation. The presence of new blood vessel formation was already detectable 2 weeks after transplantation and most importantly more evident in those animals transplanted with scaffolds preseeded with iOCT4 TECs. Quantitative PE analyses of 3D thymic structure perfusion clearly demonstrated that iOCT4 TEC-seeded scaffolds had a higher and continuous blood-perfusion than those generated with untransduced TECs. Additionally, ex vivo immunocytochemistry analyses revealed a substantial number of CD31+ endothelial cells spread in iOCT4 TEC-seeded scaffolds. These results indicate that 3% BDDGE collagen type I scaffolds could be easily perfused and colonized by

endothelial cells and suggest a potential role of iOCT4 TECs in promoting de novo vascularization after in vivo implantation. Of note, small clusters of mTECs (cytokeratin 5+) and cTECs (cytokeratin 8+) were detectable in iOCT4 TEC-seeded scaffolds starting from 2 weeks after in vivo transplantation. Notably, these cell agglomerates were not present or barely visible in transplanted scaffolds preseeded with cells different from iOCT4 TECs. Moreover, ultrasound and MRI studies performed on our 3D structures in vivo demonstrated the possibility to detect them with imaging techniques commonly applied in patients for soft tissues assessment. Both MRI and ultrasound allowed to easily distinguish the transplanted thymic structure from the surrounding soft tissue and to monitor their vascularization. Hence, MRI and US could represent useful radiological tools to monitor scaffolds engraftment in a potential future clinical application of our strategy.

Many studies have demonstrated that tissue engineered constructs failed to succeed because scaffolds were insufficiently porous, avoiding the formation of new blood vessels, or because they rapidly degraded after in vivo implantation [62]. Despite achieving good porosity and observing new blood vessel formation in our 3D thymic-like structures, we also noticed that iOCT4 TEC-seeded thymic-like organoids were rapidly degraded in vivo, impairing the growth of both iOCT4 TECs and endothelial cells, and consequently limiting their efficacy in sustaining thymopoiesis after implantation. A strong infiltration of neutrophils and macrophages, detected 2 and 4 weeks after in vivo subcutaneous transplantation, could be the major cause of the rapid core degradation. Further improvement of scaffold formulation is necessary in order to increase their in vivo persistency and could be achieved by using different methods for the crosslinking of collagen fibers that could also potentially be more appropriate for future human medical application of the 3D scaffolds [63]. Additionally, to improve the establishment of a functional and stable vascular perfusion inside the 3D structure, we are also considering functionalization of 3D scaffolds with angiogenic signals that would guarantee a local and sustained growth factor delivery ultimately leading to enhanced and sustained thymic organoids vascularization [64].

## CONCLUSION

In this study, we provided proof of principle that collagen type I scaffolds possess important features that could be exploited and further implemented for thymic tissue engineering such as biocompatibility, biodegradability, and mechanical properties to ensure cell penetration and scaffold vascularization. Additionally, we showed that gene modification, mediated by Oct4 induction, allowed the use of postnatal TECs for the formation of 3D thymic-like structures. The lack of functionality observed in immunodeficient mice after iOCT4 scaffolds transplantation could be due to the extensive colonization of the scaffold by innate immune cells of the host, in particular high number of neutrophils and macrophages. Scaffolds degradation was already visible and detectable 2 weeks after in vivo implantation, preventing any functional studies and most importantly impairing iOCT4 TEC organoids' ability to sustain de novo thymopoiesis. As a future perspective, to overcome the hurdles encountered, we might further implement the protocol by using higher numbers of TECs and exploiting alternative biomimetic

and functionalized 3D scaffolds able to support long-term in vivo persistence and thymopoietic activity of thymic organoids.

## AUTHOR CONTRIBUTIONS

I.B.: conception and design, collection and/or assembly of data, data analyses and interpretation, manuscript writing, final approval of manuscript; M.S., E.C.: provision of study material, final approval of manuscript; E.D., E.F., G.E.M., F.F.: collection and/or assembly of data, final approval of manuscript; L.P., A.S., T.C.: collection and/or assembly of data, data analyses and interpretation, final approval of manuscript; M.C., A.E., A.L., L.N.: final approval of manuscript; T.D.T., L.S.S.: provision of study material; A.T.: financial support, final approval of manuscript; G.A.H., A.V.: conception and design, financial support, manuscript writing, final approval of manuscript; M.B.: conception and design, collection and/or assembly of data, data analyses and interpretation, financial support, manuscript writing, final approval of manuscript.

## DISCLOSURE OF POTENTIAL CONFLICTS OF INTEREST

The authors indicated no potential conflicts of interest.

## DATA AVAILABILITY STATEMENT

The data that support the findings of this study are available from the corresponding author upon reasonable request.

## REFERENCES

**1** Csaba G. The immunoendocrine thymus as a pacemaker of lifespan. Acta Microbiol Immunol Hung 2016;63:139–158.

**2** Zdrojewicz Z, Pachura E, Pachura P. The thymus: A forgotten, but very important organ. Adv Clin Exp Med 2016;25:369–375.

**3** Lepletier A, Alsharif A, Chidgey AP. Inflammation and thymus ageing. Front Horm Res 2017;48:19–36.

**4** Masters AR, Haynes L, Su DM. Immune senescence: Significance of the stromal microenvironment. Clin Exp Immunol 2017;187:6–15.

**5** Majumdar S, Nandi D. Thymic atrophy: Experimental studies and therapeutic interventions. Scand J Immunol 2017;12:3218–3221.

**6** Xiao S, Shterev ID, Zhang W. Sublethal total body irradiation causes long-term deficits in thymus function by reducing lymphoid progenitors. J Immunol 2017;199:2701–2712.

**7** Dudakov J a, van den Brink MRM. Greater than the sum of their parts: Combination strategies for immune regeneration following allogeneic hematopoietic stem cell transplantation. Best Pract Res Clin Haematol 2011;24:467–476.

**8** Van Den Brink MRM, Chaudhry MS, Velardi E. Hematopoietic stem cell transplantation: Immune reconstitution after allogeneic immune reconstitution after allogeneic hematopoietic stem cell transplantation: Time to T up the thymus. J Immunol Ref 2017;198:40–46.

**9** Bredenkamp N, Nowell CS, Blackburn CC. Regeneration of the aged thymus by a single transcription factor. Development 2014;141: 1627–1637.

**10** Chaudhry MS, Velardi E, Dudakov JA. Thymus: The next (re)generation. Immunol Rev 2016;271:56–71.

**11** Chung B, Montel-Hagen A, Ge S. Engineering the human thymic microenvironment to support thymopoiesis in vivo. STEM CELLS 2014;32:2386–2396.

**12** Dudakov J a, Hanash AM, Jenq RR. Interleukin-22 drives endogenous thymic regeneration in mice. Science 2012;336:91–95.

**13** Rossi SW, Jeker LT, Ueno T. Keratinocyte growth factor (KGF) enhances postnatal T-cell development via enhancements in proliferation and function of thymic epithelial cells. Blood 2007;109:3803–3811.

**14** Goldberg GL, Dudakov JA, Reiseger JJ. Sex steroid ablation enhances immune reconstitution following cytotoxic antineoplastic therapy in young mice. J Immunol 2010; 184:6014–6024.

**15** Mittelstadt PR, Monteiro JP, Ashwell JD. Thymocyte responsiveness to endogenous glucocorticoids is required for immunological fitness. J Clin Invest 2012;122:2384–2394.

**16** Markert ML, Devlin BH, Alexieff MJ. Review of 54 patients with complete DiGeorge anomaly enrolled in protocols for thymus transplantation: Outcome of 44 consecutive transplants. Blood 2007;109:4539–4547.

**17** Davies EG, Cheung M, Gilmour K. Thymus transplantation for complete DiGeorge syndrome: European experience. J Allergy Clin Immunol 2016;140:1660–1670.e16.

**18** Blackburn CC, Manley NR. Developing a new paradigm for thymus organogenesis. Nat Rev Immunol 2004;4:278–289.

**19** Schmitt A, Csiki R, Tron A. Optimized protocol for whole organ decellularization. Eur J Med Res 2017;22:31.

**20** Takebe T, Zhang B, Radisic M. Synergistic engineering: Organoids meet organs-on-a-chip. Cell Stem Cell 2017;21:297–300.

**21** Poznansky MC, Evans RH, Foxall RB. Efficient generation of human T cells from a tissue-engineered thymic organoid. Nat Biotechnol 2000;18:729–734.

**22** Fan Y, Tajima A, Goh SK. Bioengineering thymus organoids to restore thymic function and induce donor-specific immune tolerance to allografts. Mol Ther 2015;23:1262–1277.

**23** Seach N, Hammett M, Chidgey A. Isolation, characterization, and reaggregate culture of thymic epithelial cells. Methods Mol Biol 2013;945:251–272.

**24** Inami Y, Yoshikai T, Ito S. Differentiation of induced pluripotent stem cells to thymic epithelial cells by phenotype. Immunol Cell Biol 2011;89:314–321.

**25** Parent AV, Russ HA, Khan IS. Generation of functional thymic epithelium from human embryonic stem cells that supports host T cell development. Cell Stem Cell 2013;13:219–229.

**26** Sun X, Xu J, Lu H. Directed differentiation of human embryonic stem cells into thymic epithelial progenitor-like cells reconstitutes the thymic microenvironment in vivo. Cell Stem Cell 2013;13:230–236.

**27** Pinto S, Schmidt K, Egle S. An organotypic coculture model supporting proliferation and differentiation of medullary thymic epithelial cells and promiscuous gene expression. J Immunol 2013;190:1085–1093.

**28** Tajima A, Liu W, Pradhan I. Bioengineering mini functional thymic units with EAK16-II/EAKIIH6 self-assembling hydrogel. Clin Immunol 2015;160:82–89.

**29** Seach N, Ph D, Mattesich M. Vascularized tissue engineering mouse chamber model supports thymopoiesis of ectopic thymus grafts. Tissue Eng Part C Methods 2010;16:543–551.

**30** El-Jawhari JJ, Sanjurjo-Rodríguez C, Jones E. Collagen-containing scaffolds enhance attachment and proliferation of non-cultured bone marrow multipotential stromal cells. J Orthop Res 2016;34:597–606.

**31** Hadjizadeh A, Doillon CJ. Directional migration of endothelial cells towards angiogenesis using polymer fibres in a 3D co-culture system. J Tissue Eng Regen Med 2010;4:524–531.

**32** Krishnakumar GS, Gostynska N, Campodoni E. Ribose mediated crosslinking of collagen-hydroxyapatite hybrid scaffolds for

bone tissue regeneration using biomimetic strategies. Mater Sci Eng C 2017;77:594–605.

**33** Gostynska N, Krishnakumar G, Campodoni E. 3D porous collagen scaffolds reinforced by glycation with ribose for tissue engineering application. Biomed Mater 2017;12:055002.

**34** Van Den Hurk M, Kenis G, Bardy C. Transcriptional and epigenetic mechanisms of cellular reprogramming to induced pluripotency. Epigenomics 2016;8:1131–1149.

**35** Hochedlinger K, Yamada Y, Beard C. Ectopic expression of Oct-4 blocks progenitor-cell differentiation and causes dysplasia in epithelial tissues. Cell 2005;121:465–477.

**36** De Palma M, Naldini L. Transduction of a gene expression cassette using advanced generation lentiviral vectors. Methods Enzymol 2002; 346:514–529.

**37** Castiello MC, Scaramuzza S, Pala F. B-cell reconstitution after lentiviral vector-mediated gene therapy in patients with Wiskott–Aldrich syndrome. J Allergy Clin Immunol 2015;136: 692.e2–702.e2.

**38** Sandri M, Filardo G, Kon E. Fabrication and pilot in vivo study of a collagen-BDDGE-elastin core-shell scaffold for tendon regeneration. Front Bioeng Biotechnol 2016;4:52.

**39** Nicoletti A, Fiorini M, Paolillo J. Effects of different crosslinking conditions on the chemical–physical properties of a novel bio-inspired composite scaffold stabilised with 1,4-butanediol diglycidyl ether (BDDGE). J Mater Sci Mater Med 2013;24:17–35.

**40** Shankar KG, Gostynska N, Montesi M. Investigation of different cross-linking approaches on 3D gelatin scaffolds for tissue engineering application: A comparative analysis. Int J Biol Macromol 2017;95:1199–1209.

**41** Arora A, Kothari A, Katti DS. Pore orientation mediated control of mechanical behavior of scaffolds and its application in cartilage-mimetic scaffold design. J Mech Behav Biomed Mater 2015;51:169–183.

**42** Loh QL, Choong C. Three-dimensional scaffolds for tissue engineering applications: Role of porosity and pore size. Tissue Eng Part B Rev 2013;19:485–502.

**43** Davidenko N, Schuster CF, Bax DV. Control of crosslinking for tailoring collagen-based scaffolds stability and mechanics. Acta Biomater 2015;25:131–142.

**44** Needles A, Arditi M, Rognin NG. Nonlinear contrast imaging with an array-based micro-ultrasound system. Ultrasound Med Biol 2010;36:2097–2106.

**45** Lannes-Vieira J, Dardenne M, Savino W. Extracellular matrix components of the mouse thymus microenvironment: Ontogenetic studies and modulation by glucocorticoid hormones. J Histochem Cytochem 1991;39:1539–1546.

**46** Savino W, Mendes-da-Cruz DA, Smaniotto S. Molecular mechanisms governing thymocyte migration: Combined role of chemokines and extracellular matrix. J Leukoc Biol 2004;75:951–961.

**47** Hun M, Barsanti M, Wong K. Native thymic extracellular matrix improves in vivo thymic organoid T cell output, and drives in vitro thymic epithelial cell differentiation. Biomaterials 2017;118:1–15.

**48** Krishnakumar GS, Gostynska N, Dapporto M. Evaluation of different crosslinking agents on hybrid biomimetic collagen-hydroxyapatite composites for regenerative medicine. Int J Biol Macromol 2018;106:739–748.

**49** Meireles C, Ribeiro AR, Pinto RD. Thymic crosstalk restrains the pool of cortical thymic epithelial cells with progenitor properties. Eur J Immunol 2017;47:958–969.

**50** Osada M, Singh VJ, Wu K. Label retention identifies a multipotent mesenchymal stem cell-like population in the postnatal thymus. PLoS One 2013;8:e83024.

**51** Žuklys S, Handel A, Zhanybekova S. Foxn1 regulates key target genes essential for T cell development in postnatal thymic epithelial cells. Nat Immunol 2016;17:1206–1215.

**52** Le Campion A, Gagnerault MC, Auffray C. Lymphopenia-induced spontaneous T-cell proliferation as a cofactor for autoimmune disease development. Blood 2009;114:1784–1793.

**53** O'Brien FJ. Biomaterials & scaffolds for tissue engineering. Mater Today 2011;14:88–95.

**54** Jenkinson EJ, Franchi LL, Kingston R. Effect of deoxyguanosine on lymphopoiesis in the developing thymus rudiment in vitro: Application in the production of chimeric thymus rudiments. Eur J Immunol 1982;12: 583–587.

**55** Jenkinson EJ, Anderson G, Owen JJ. Studies on T cell maturation on defined thymic stromal cell populations in vitro. J Exp Med 1992;176:845–853.

**56** Schmitt TM, Zúñiga-Pflücker JC. Induction of T cell development from hematopoietic progenitor cells by delta-like-1 in vitro. Immunity 2002;17:749–756.

**57** Beaudette-Zlatanova BC, Knight KL, Zhang S. A human thymic epithelial cell culture system for the promotion of lymphopoiesis from hematopoietic stem cells. Exp Hematol 2011;39:570–579.

**58** Mou Y, Yue Z, Wang X. OCT4 remodels the phenotype and promotes angiogenesis of HUVECs by changing the gene expression profile. Int J Med Sci 2016; 13:386–394.

**59** Rode I, Martins VC, Küblbeck G. Foxn1 protein expression in the developing, aging, and regenerating thymus. J Immunol 2015; 195:5678–5687.

**60** Alunno A, Bistoni O, Bartoloni Bocci E. IL-17-producing double-negative T cells are expanded in the peripheral blood, infiltrate the salivary gland and are partially resistant to corticosteroid therapy in patients with Sjögren's syndrome. Reumatismo 2013; 65:192–198.

**61** D'Acquisto F, Crompton T. CD3+CD4 −CD8− (double negative) T cells: Saviours or villains of the immune response? Biochem Pharmacol 2011;82:333–340.

**62** Phelps EA, Garcia AJ. Update on therapeutic vascularization strategies. Regen Med 2009;4:65–80.

**63** Reddy N, Reddy R, Jiang Q. Crosslinking biopolymers for biomedical applications. Trends Biotechnol 2015;33:362–369.

**64** Jay SM, Shepherd BR, Bertram JP. Engineering of multifunctional gels integrating highly efficient growth factor delivery with endothelial cell transplantation. FASEB J 2008; 22:2949–2956.

See www.StemCellsTM.com for supporting information available online.